

# METAL INPAINTING IN CBCT PROJECTIONS USING SCORE-BASED GENERATIVE MODEL

Siyuan Mei, Fuxin Fan, Andreas Maier

Friedrich-Alexander-Universität Erlangen-Nürnberg  
Pattern Recognition Lab  
Erlangen, Germany

## ABSTRACT

During orthopaedic surgery, the inserting of metallic implants or screws are often performed under mobile C-arm systems. Due to the high attenuation of metals, severe metal artifacts occur in 3D reconstructions, which degrade the image quality greatly. To reduce the artifacts, many metal artifact reduction algorithms have been developed and metal inpainting in projection domain is an essential step. In this work, a score-based generative model is trained on simulated knee projections and the inpainted image is obtained by removing the noise in conditional resampling process. The result implies that the inpainted images by score-based generative model have more detailed information and achieve the lowest mean absolute error and the highest peak-signal-to-noise-ratio compared with interpolation and CNN based method. Besides, the score-based model can also recover projections with big circular and rectangular masks, showing its generalization in inpainting task.

**Index Terms**— Knee projection inpainting, score-based generative model, unsupervised learning

## 1. INTRODUCTION

The mobile C-arm systems are frequently used in interventional surgery currently, which supports the accurate placement of metallic implants or screws. However, some physical effects like photon starvation and beam hardening occur when x-rays pass through metals, resulting the bright and dark streak artifacts, which reduce the quality of the reconstructed image [1]. The conventional metal artifacts reduction (MAR) algorithms tackle the problem by sinogram completion [2, 3] and iterative reconstruction [4, 5]. Deep learning based methods are also applied in MAR [6, 7, 8, 9, 10] and the models are trained on paired data in the supervised way. For the C-arm system, since only the central slice in cone-beam geometry can be represented as sinogram and other artifacts like truncation artifacts also exist in reconstructions, image inpainting in projection domain is the feasible way for MAR.

Score-based generative models are applied in computer vision recently [11, 12] and with the mechanism of stepwise

noise perturbation and removal, they have shown superiority over generative adversarial networks [13]. Such models are successfully applied in image inpainting task [11, 14]. In Ref. [14], a score-based generative model called RePaint is trained and it can generate restored image with high fidelity under different masks. Besides, score-based generative models are used in the field of medical imaging processing, such as CT and MRI reconstruction [15, 16]. Inspired by the research above, a score-based model is trained on knee projections and this is the first study to apply such model in metal inpainting in CBCT projections.

## 2. MATERIALS AND METHOD

### 2.1. Score-based generative models

Score-based generative models through stochastic differential equation (SDE) consist of three steps: perturbation process, reverse process and resampling. In the perturbation process, the original image  $x_0$  is perturbed with a stochastic process to construct a continuous diffusion process  $x_t$ , where  $t \in [0, 1]$ . The perturbation process by SDE has the following form

$$dx_t = \mathbf{f}(x_t, t)dt + g(t)dw_t, \quad t \in [0, 1], \quad (1)$$

where  $\mathbf{f}(x, t)$  is the drift coefficient,  $g(t)$  is the diffusion coefficient and  $w_t$  denotes a standard Wiener process. Depending on the change of variance during the perturbation process, SDEs are clarified into variance exploding (VE), variance preserving (VP) and sub VP SDE. In this paper, VE SDE is used, which has the form of

$$\mathbf{f} = \mathbf{0}, g = \sqrt{\frac{d[\sigma^2(t)]}{dt}}, \quad (2)$$

$$\sigma(t) = \sigma(0)\left(\frac{\sigma(1)}{\sigma(0)}\right)^t, \quad t \in [0, 1], \quad (3)$$

where  $\sigma(t) > 0$  is increasing with the increment of  $t$ . Then the diffusion process  $x_t$  at time point  $t$  can be obtained by

$$x_t = x_0 + [\sigma^2(t) - \sigma^2(0)]\mathbf{I}, \quad (4)$$

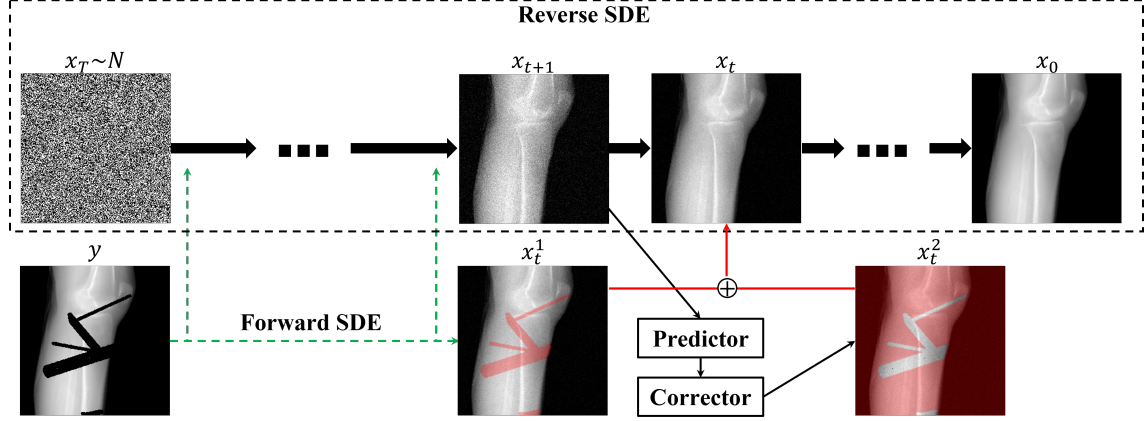


Fig. 1. The illustration of the resampling process for projection inpainting.

where  $\mathbf{I}$  is a normal distribution. The reverse process follows the equation of reverse-time SDE

$$d\mathbf{x}_t = [\mathbf{f}(\mathbf{x}_t, t)dt - g(t)^2 \nabla_{\mathbf{x}_t} \log p_t(\mathbf{x}_t)] + g(t)d\bar{\mathbf{w}}_t, t \in [0, 1], \quad (5)$$

where  $\nabla_{\mathbf{x}_t} \log p_t(\mathbf{x}_t)$  is the score function of  $p_t(\mathbf{x}_t)$  and  $\bar{\mathbf{w}}_t$  denotes the reverse Wiener process. Following the reverse process, the perturbed image will be restored gradually. In the case of VE SDE which is used in this paper, the Eq. 6 can be rewritten as

$$d\mathbf{x}_t = -\frac{d[\sigma^2(t)]}{dt} \nabla_{\mathbf{x}_t} \log p_t(\mathbf{x}_t) + \frac{d[\sigma^2(t)]}{dt} d\bar{\mathbf{w}}_t, \quad t \in [0, 1]. \quad (6)$$

Then  $\mathbf{x}_t$  in the reverse process has the form of

$$\mathbf{x}_t = \mathbf{x}_{t+\Delta t} - d\mathbf{x}_{t+\Delta t}. \quad (7)$$

For projection inpainting, the missing pixels in the metal area should be restored and the pixels in the background serve as conditional information in the resampling process. The pipeline for projection inpainting is shown in Fig. 1. We denote the projection to be inpainted as  $\mathbf{y}$  and the binary metal mask with ones in the background as  $\mathbf{m}$ .  $\mathbf{x}_t^1$  is obtained by forward SDE and has the form of

$$\mathbf{x}_t^1 = \mathbf{y} + [\sigma^2(t) - \sigma^2(0)]\mathbf{I}, \quad (8)$$

and it provides the background information.  $\mathbf{x}_t^2$  follows reverse SDE and is written as

$$\mathbf{x}_t^2 = \mathbf{x}_{t+1} - d\mathbf{x}_{t+1}, \quad (9)$$

and it predicts the inpainted pixels. Then the restored projection  $\mathbf{x}_t$  at time point  $t$  can be obtained as

$$\mathbf{x}_t = \mathbf{x}_t^1 \odot \mathbf{m} + \mathbf{x}_t^2 \odot (1 - \mathbf{m}), \quad (10)$$

where  $\odot$  means pixelwise multiplication.

## 2.2. Data generation

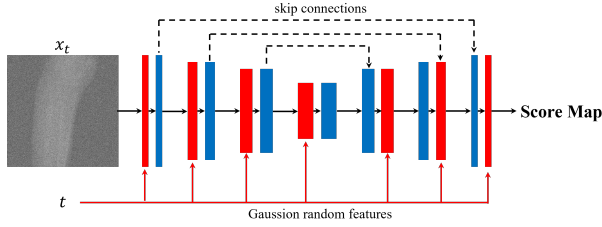
The knee CT volumes are selected from the whole body CT volumes from the SICAS medical image repository [17]. In total, there are 50 volumes with single leg for each of them and all volumes are rescaled to a voxel side length of 0.5 mm. All the volumes are forward projected to generate projections by CONRAD [18]. The parameters for defining the C-arm trajectory are listed in Tab. 1. 3000 projections are generated and 2700 of them are used for model training and 300 projections are used for test. To generate metal masks, some implants like K-wires, screws, plates with holes are drawn using the software AutoCAD. Then these implants are randomly selected and placed in different 3D volumes. The metal masks are obtained by forward projecting these multi-metal volumes under the same parameters shown in Tab. 1.

Table 1. Parameters for the mobile C-arm system.

Parameter	Value
Scan angular range	360°
Incremental Angular step	6°
Source-to-detector distance	1164 mm
Source-to-isocenter distance	622 mm
Detector Size	256 × 256
Detector pixel size	1.16 mm × 1.16 mm

## 2.3. Network Structures

Since the mask pyramid network (MPN) from Ref. [7] has good performance in projection inpainting, its results are used for comparison. The projection to be inpainted and the corresponding metal mask are the inputs for MPN, both of which



**Fig. 2.** The network structure for the score-based generative model.

have the size of  $256 \times 256$ . According to Ref. [11], the network structure for the score-based generative model has high flexibility. As shown in Fig. 2, the structure of MPN without downsampling layers from metal mask serves as the backbone for the score-based generative model in this work. Besides, the Gaussian random features [19] are generated at time step  $t$  and these features are summed up with the corresponding blocks from the network, which are labeled in red in Fig. 2. For the defined VE SDE in this work, the minimum and maximum variances are 0.01 and 128, respectively. During the resampling process, the image of gaussian noise with variance of  $\sigma(1)$  is the initializer and the inpainted projection is generated by predictor-corrector (PC) resampler for 1000 steps. All experiments are conducted on Nvidia A100 GPU.

#### 2.4. Hyperparameter optimization

Some hyperparameters in the sampling process are considered, including the signal-to-noise ratio (SNR)  $\eta$  for corrector, and the number of discretization steps  $N$  for reverse-time SDE. SNR determines the step size  $\epsilon$  in Langevin dynamics, and  $N$  corresponds to the noise scales. The quantitative results for 300 projections with metal masks under *ancestral sampling* predictor and *Langevin* corrector are listed in Tab. 2. It demonstrates that  $\eta = 0.4$  (with star remarked) can achieve better performance than others. Time consumption is an important issue in clinical applications. According to Tab. 2,  $N$  is proportional to time usage, and it has limited performance improvement from 1000 to 2000 steps. Therefore, the parameters in our experiments are chosen as  $\eta = 0.4$ ,  $N=1000$ .

### 3. RESULTS AND DISCUSSION

In this work, result evaluation is compared among inpainted projections generated by interpolation, MPN and the score-based generative model. Three representative inpainted projections with different metal masks are shown in Fig. 3. From Fig. 3 (a1) to (c1), more pixels are missing. The interpolation method relies on the intensity of existing pixels outside the metal area. Therefore, the inpainted projections by interpolation method have no semantic connections to the bones or

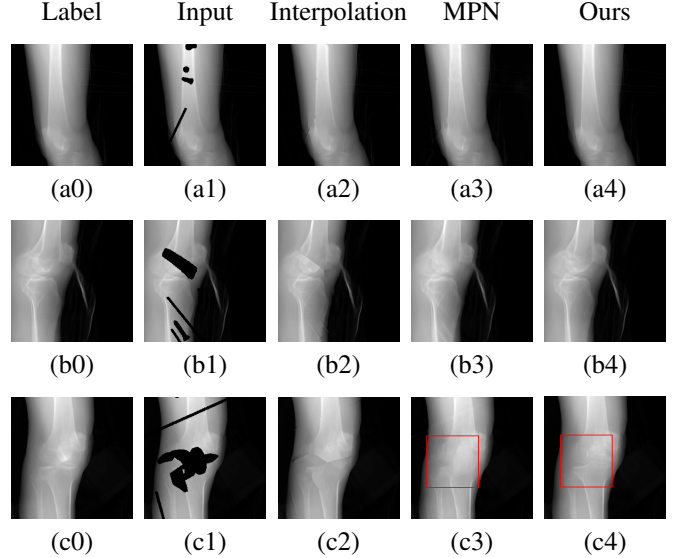


**Fig. 3.** The inpainting results under different metal masks.

soft tissue, as shown in Fig. 3 (a2)-(c2). For the perspective of semantic performance, the inpainted projections by MPN can restore more details in the metal area. However, when the size of metal area increases, the prediction gets blurred, which can be observed inside the red boxes in Fig. 3 (c3). In the same region in Fig. 3 (c4), the inpainted projections by the score-based generative model have more detailed information. The quantitative evaluation results for all 300 projections with metal masks are shown in Tab. 3. The score-based generative model has the lowest mean absolute error (MAE) of 0.015 in metal regions and the highest mean peak-signal-to-noise-ratio (PSNR) of 43.00.

Except for the metal masks, some circular and rectangular masks are also generated to test the generalization of these methods. As shown in Fig. 4 (a1)-(c1), a circle, horizontal and vertical rectangles mask out the leg projections. The results by interpolation method have more discontinuity. By giving blurring predictions with distinct boundaries, MPN is not able to recover the missing pixels properly in all three cases. Although the score-based generative model also has degraded performance with blurry area in Fig. 4 (a4) and incorrect bone in Fig. 4 (c4), this model gives the best predictions among all methods. The quantitative results for 300 projections with circular or rectangular masks are listed in Tab. 3. The diameter of circles during test vary from 20 pixels to 60 pixels. The width of horizontal or vertical rectangle has the range of 20–50 pixels. In the case of rectangular masks, MPN has the largest MAE as well as the lowest PSNR. According to Tab. 3, the score-based generative model has the best results in all cases.

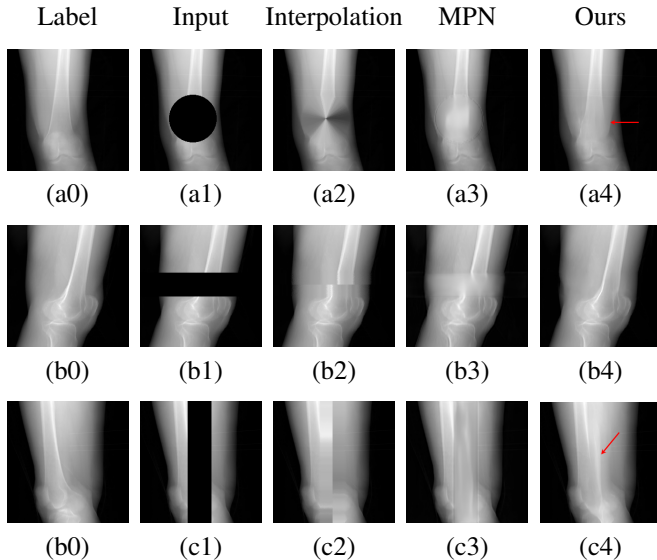
MPN is trained by supervised learning, which needs the paired data of inputs and labels. This is the reason that it fails

**Table 2.** Ablation study on SNR and sampling steps under same PC sampler.

Metric	$N=500$		$N=1000$		$N=2000$	
	MAE	PSNR	MAE	PSNR	MAE	PSNR
$\eta=0.20$	0.0197	40.85	0.0172	41.99	0.0154	42.74
$\eta=0.40^*$	0.0161	42.39	0.0148	43.00	0.0146	43.07
$\eta=0.60$	0.0172	41.94	0.0178	41.67	0.0201	40.82
time per slice(s)	2.50		4.38		9.79	

**Table 3.** Quantitative results comparison.

Metric	Interpolation		MPN		Score-based model	
	MAE	PSNR	MAE	PSNR	MAE	PSNR
Metal mask	0.031	35.92	0.025	39.22	0.015	43.00
Circle	0.070	31.50	0.039	37.89	0.026	41.31
Horizontal rectangle	0.014	41.11	0.019	40.10	0.009	45.51
Vertical rectangle	0.064	32.73	0.072	30.33	0.035	37.44

**Fig. 4.** The inpainting results under circular and rectangular masks.

to give the correct inpainting predictions when the projections are masked out by masks which differ a lot to the training data. The score-based generative model learns the score function at different time point and it tackles the inpainting task in an unsupervised way. The background of projections guide the model to predict the missing pixels step by step in the resampling process. The metal masks in clinic have more combinations and the training data can never guarantee such diversity. Therefore, considering the robustness and generalization ability of these methods, the score-based generative model is more reliable for clinical use. However, the score-

based model takes longer time because of thousands steps of resampling. The future work needs to solve this problem and projections with higher resolution should be used for clinical use.

#### 4. CONCLUSION

This work applies the score-based generative model in metal inpainting for knee CBCT projections. By predicting more detailed information under metal masks, the proposed unsupervised method has the best performance, which is supposed to benefit MAR algorithms. What is more, the score-based generative model is able to restore the knee projections when faced with bigger circular and rectangular masks, showing its robustness in CBCT projection inpainting task.

#### 5. COMPLIANCE WITH ETHICAL STANDARDS

This is a numerical simulation study for which no ethical approval was required.

#### 6. ACKNOWLEDGMENTS

The concepts and information presented in this paper are based on research and are not commercially available.

#### 7. REFERENCES

- [1] Masaki Katsura, Jiro Sato, Masaaki Akahane, Akira Kunitatsu, Osamu Abe, et al., "Current and novel techniques for metal artifact reduction at ct: practical guide for radiologists," *Radiographics*, vol. 38, no. 2, pp. 450–461, 2018.

- [2] Esther Meyer, Rainer Raupach, Michael Lell, Bernhard Schmidt, and Marc Kachelrieß, “Normalized metal artifact reduction (nmar) in computed tomography,” *Medical physics*, vol. 37, no. 10, pp. 5482–5493, 2010.
- [3] Esther Meyer, Rainer Raupach, Michael Lell, Bernhard Schmidt, and Marc Kachelrieß, “Frequency split metal artifact reduction (fsmar) in computed tomography,” *Medical physics*, vol. 39, no. 4, pp. 1904–1916, 2012.
- [4] Ge Wang, Donald L Snyder, Joseph A O’Sullivan, and Michael W Vannier, “Iterative deblurring for ct metal artifact reduction,” *IEEE transactions on medical imaging*, vol. 15, no. 5, pp. 657–664, 1996.
- [5] Xiaomeng Zhang, Jing Wang, and Lei Xing, “Metal artifact reduction in x-ray computed tomography (ct) by constrained optimization,” *Medical physics*, vol. 38, no. 2, pp. 701–711, 2011.
- [6] Yanbo Zhang and Hengyong Yu, “Convolutional neural network based metal artifact reduction in x-ray computed tomography,” *IEEE transactions on medical imaging*, vol. 37, no. 6, pp. 1370–1381, 2018.
- [7] Haofu Liao, Wei-An Lin, Zhimin Huo, Levon Vogelsang, William J Sehnert, S Kevin Zhou, and Jiebo Luo, “Generative mask pyramid network for ct/cbct metal artifact reduction with joint projection-sinogram correction,” in *International Conference on Medical Image Computing and Computer-Assisted Intervention*. Springer, 2019, pp. 77–85.
- [8] Tristan M Gottschalk, Björn W Kreher, Holger Kunze, and Andreas Maier, “Deep learning based metal inpainting in the projection domain: Initial results,” in *International Workshop on Machine Learning for Medical Image Reconstruction*. Springer, 2019, pp. 125–136.
- [9] Tao Wang, Wenjun Xia, Yongqiang Huang, Huaiqiang Sun, Yan Liu, Hu Chen, Jiliu Zhou, and Yi Zhang, “Dual-domain adaptive-scaling non-local network for ct metal artifact reduction,” in *International Conference on Medical Image Computing and Computer-Assisted Intervention*. Springer, 2021, pp. 243–253.
- [10] Hong Wang, Yuexiang Li, Nanjun He, Kai Ma, Deyu Meng, and Yefeng Zheng, “Dicdnet: Deep interpretable convolutional dictionary network for metal artifact reduction in ct images,” *IEEE Transactions on Medical Imaging*, vol. 41, no. 4, pp. 869–880, 2021.
- [11] Yang Song, Jascha Sohl-Dickstein, Diederik P Kingma, Abhishek Kumar, Stefano Ermon, and Ben Poole, “Score-based generative modeling through stochastic differential equations,” in *International Conference on Learning Representations*, 2020.
- [12] Jonathan Ho, Ajay Jain, and Pieter Abbeel, “Denoising diffusion probabilistic models,” *Advances in Neural Information Processing Systems*, vol. 33, pp. 6840–6851, 2020.
- [13] Prafulla Dhariwal and Alexander Nichol, “Diffusion models beat gans on image synthesis,” *Advances in Neural Information Processing Systems*, vol. 34, pp. 8780–8794, 2021.
- [14] Andreas Lugmayr, Martin Danelljan, Andres Romero, Fisher Yu, Radu Timofte, and Luc Van Gool, “Re-paint: Inpainting using denoising diffusion probabilistic models,” in *Proceedings of the IEEE/CVF Conference on Computer Vision and Pattern Recognition*, 2022, pp. 11461–11471.
- [15] Yang Song, Liyue Shen, Lei Xing, and Stefano Ermon, “Solving inverse problems in medical imaging with score-based generative models,” in *International Conference on Learning Representations*, 2021.
- [16] Hyungjin Chung and Jong Chul Ye, “Score-based diffusion models for accelerated mri,” *Medical Image Analysis*, p. 102479, 2022.
- [17] Michael Kistler, Serena Bonaretti, Marcel Pfahrer, Roman Niklaus, Philippe Büchler, et al., “The virtual skeleton database: an open access repository for biomedical research and collaboration,” *Journal of medical Internet research*, vol. 15, no. 11, pp. e2930, 2013.
- [18] Andreas Maier, Hannes G Hofmann, Martin Berger, Peter Fischer, Chris Schwemmer, Haibo Wu, Kerstin Müller, Joachim Hornegger, Jang-Hwan Choi, Christian Riess, et al., “Conrad—a software framework for cone-beam imaging in radiology,” *Medical physics*, vol. 40, no. 11, pp. 111914, 2013.
- [19] Matthew Tancik, Pratul Srinivasan, Ben Mildenhall, Sara Fridovich-Keil, Nithin Raghavan, Utkarsh Singhal, Ravi Ramamoorthi, Jonathan Barron, and Ren Ng, “Fourier features let networks learn high frequency functions in low dimensional domains,” *Advances in Neural Information Processing Systems*, vol. 33, pp. 7537–7547, 2020.